crystals

MDPI

Article

SrNi(VO_4)(OH): The High-Temperature Hydrothermal Synthesis and Magnetic Properties of an Adelite-Descloizite-Type Structure

Liurukara D. Sanjeewa [1,2,*], Tiffany M. Smith Pellizzeri [3], Colin D. McMillen [4], Keith Taddei [5], Thomas Heitmann [1,6], Helmut Kaiser [1,6] and Joseph W. Kolis [4,*]

1 University of Missouri Research Reactor (MURR), University of Missouri, Columbia, MO 65211, USA
2 Department of Chemistry, University of Missouri, Columbia, MO 65211, USA
3 Department of Chemistry and Biochemistry, Eastern Illinois University, Charleston, IL 61920, USA
4 Department of Chemistry, Center for Optical Materials Science and Engineering Technologies (COMSET), Clemson University, Clemson, SC 29634, USA
5 Neutron Scattering Division, Oak Ridge National Laboratory, Oak Ridge, TN 37831, USA
6 Department of Physics and Astronomy, University of Missouri, Columbia, MO 65211, USA
* Correspondence: sanjeewal@missouri.edu (L.D.S.); kjoseph@clemson.edu (J.W.K.)

Abstract: Single crystals of a new transition metal adelite-descloizite-type structure were synthesized using a high temperature (580 °C) high-pressure hydrothermal technique. Single crystal X-ray diffraction and energy dispersive X-ray analysis (EDX) were used to investigate the structure and elemental composition, respectively. SrNi(VO_4)(OH) crystallizes in an acentric orthorhombic crystal system in the space group $P2_12_12_1$ (no. 19); $Z = 4$, $a = 5.9952(4)$ Å, $b = 7.5844(4)$ Å, $c = 9.2240(5)$ Å. The structure is comprised of a Ni–O–V framework where Sr^{2+} ions reside inside the channels. Single-crystal magnetic measurements display a significant anisotropy in both temperature- and field-dependent data. The temperature dependent magnetic measurement shows antiferromagnetic behavior at T_N~8 K. Overall, the magnetic properties indicate the presence of competing antiferromagnetic and ferromagnetic interactions of SrNi(VO_4)(OH).

Keywords: hydrothermal; vanadates; nickel(II); antiferomagnetism

Citation: Sanjeewa, L.D.; Pellizzeri, T.M.S.; McMillen, C.D.; Taddei, K.; Heitmann, T.; Kaiser, H.; Kolis, J.W. SrNi(VO_4)(OH): The High-Temperature Hydrothermal Synthesis and Magnetic Properties of an Adelite-Descloizite-Type Structure. *Crystals* **2022**, *12*, 1360. https://doi.org/10.3390/cryst12101360

Academic Editors: Jacek Krawczyk, Wlodzimierz Bogdanowicz and Bo Liu

Received: 26 August 2022
Accepted: 21 September 2022
Published: 26 September 2022

1. Introduction

The vanadate oxyanion $(VO_4)^{3-}$ displays a remarkable ability to form new solid phases with first row transition metal ions. The tetrahedral group shows considerable flexibility in coordinating and bridging the transition metal cations in multiple environments and linking formats [1,2]. Vanadate tetrahedra bear structural and electronic similarities to corresponding phosphate groups, but several factors make them unique in their chemistry and properties. Vanadium has the ability to adopt lower oxidation states as well as to form polyvanadate building blocks that dramatically enhance the structural variations that can be observed [3]. One particularly significant aspect of the vanadate group is its magnetic properties. The vanadate tetrahedra can form low dimensional frustrated spin lattices [4–8]. Furthermore, the presence of vacant *d*-orbitals in the bridging group leads to considerable variation in coupling constants. These various factors combine to lead to a series of solids with very interesting magnetic properties [9–11].

Recently we found that the high temperature hydrothermal method is an excellent route to transition metal vanadates [12–23]. Typically we perform the hydrothermal crystal growth reactions between 500 and 700 °C. Although these temperatures are hot for water, they are quite low for typical metal oxide crystal growth since the metal oxides are usually refractory and require much higher temperatures to react. It is also often difficult to grow single crystals of such oxides because they can be unstable in such higher temperatures. The vanadates provide an excellent example of that issue, as the V^{5+} state tends to become

unstable forming lattice defects and partially reduced vanadium sites as epitomized by the case of the single crystal growth of YVO_4 [24,25]. In the relatively low temperature hydrothermal growth method, the metal oxidation states are generally maintained well. This effect has been observed by others as well [26].

The ability to grow a rich variety of complex new phases as large, high quality single crystals is important in the study of new magnetic materials. These crystals can often be of size sufficient to acquire single crystal neutron diffraction and scattering measurements and provide detailed magnetic structural data and this is particularly important for the study of systems with very complex magnetic structures. The growth of large single crystals is also important in that they enable the orientation of the crystals in magnetic fields which is essential for the detailed study of low dimensional systems with anisotropic magnetic behavior.

We are currently concentrating our magnetic studies on three general families of low dimensional structures, namely the 1-D brackebuschites, ($E_2M(VO_4)_2(OH)$ where E = divalent metal cation, M = trivalent metal cation) [13], the 1-D descloizites ($EM(VO_4)(OH)$ where E, M = divalent metal cations) [14,15] and the 2-D glaserites $A_2EM(VO_4)_2$. (A = alkali cation, E, M = divalent metal cations) [17,27,28]. All these classes represent examples of low dimensional chains or layers of vanadate-bridged first row transition metal ions. They are also representatives of fairly extensive mineral classes that are amenable to substitution by a variety of isolectronic metal ions. Perhaps most importantly they all form quite large high-quality single crystals from hydrothermal solutions enabling the investigation of single crystal magnetic and neutron studies. Moreover, over the years, a special attention has been devoted to 1-D magnetic systems due to their strong quantum character. Particular attention has been drawn to several new classes of 1-D systems and notable among them are mixed alkaline earth metal vanadates and silicates, $AEM_2V_2O_8$, (AE = Sr, Ba; M = Mn, Co, Cu), $BaM_2Si_2O_7$ (M = Mn, Co, Cu), respectively [29–34]. In this context, $AEM_2V_2O_8$ series are of particular interest since different spins states can be realized depending upon the transition metal ions. Additionally, $AEM_2V_2O_8$ structures exhibit a strong anisotropy and some degree of magnetic frustration [29–32]. Pyroxene, AMX_2O_6 (A = alkali ion, M = Ti, V, Cr, Mn, Fe; X = Si, Ge) is another diverse class of 1-D compounds which inherit a unique zigzag 1-D magnetic chains [35,36]. These compounds also display extremely rich magnetic properties ranging from spin-Peierls to perfect Haldane-chain magnetism depending upon the alkali-cation and transition metal ions. Furthermore, pyroxene structures are presently attracting considerable attention due to the existence of multiferroic properties.

In this paper we extend our study of the adelite-descloizite class of compounds $ATM(VO_4)(OH)$ where A is an alkaline earth ion and TM is a divalent transition metal. It has a low dimensional structure whereby the divalent transition metal ion is in an octahedral coordination environment, edge-bridging to form infinite 1-D chains [14,15]. The vanadate groups serve as bridging groups within the chains, and the hydroxide also forms one of the edge bridging groups. There is considerable chemical flexibility in the system regarding the identity of the divalent metal center resulting in a fairly broad class of materials. Although the structure has been known in the mineralogical world for some time, its physical properties have not been investigated in detail until recently. One issue, of course, is that the natural mineral samples are rarely suitable for detailed physical property measurements because they invariably contain impurities and the thermal and chemical history of the sample is unknown [37]. Recently however hydrothermal routes to manmade samples of mineral types of satisfactory size and purity have been developed and this opened the opportunity to study a wide range of mineralogically inspired structure types [12]. The 1-D adelite-descloizite mineral is an ideal system on which to perform detailed magnetic studies. It was found that a range of magnetic values could be introduced including $S = 5/2$, (Mn^{2+}) and $S = 3/2$ (Co^{2+}) [14,15]. We now take the opportunity to exploit the synthetic flexibility of this adelite-descloizite structure to examine another $S = 1$ member of this series. In this paper we describe the rational synthesis and single crystal growth of $SrNi(VO_4)(OH)$ system along with detailed magnetic study.

2. Experimental Section

2.1. Hydrothermal Crystal Growth of SrNi(VO$_4$)(OH)

All hydrothermal reactions were performed at 580 °C in 2.5-in. long silver ampules with an outer diameter of 1/4 in. Approximately, 0.2 g of reactants (0.0411 g of SrO, 0.0148 g of NiO and 0.1441 g of V_2O_5) were mixed in a molar ratio of 1:1: 3 of SrO, NiO and V_2O_5 with 0.4 mL of 5 M CsOH. The silver ampoules were welded after loading the components and the welded silver ampules were placed in Tuttle autoclave filled with water to provide suitable counter pressure. The autoclaves were heated to the desired temperature for 6–7 days. After the reaction period, brown column crystals (Figure 1a) were retrieved from the silver ampoules by washing the entire product with deionized water using a suction filtration method. The chemicals used in this study: SrO (Alfa Aesar, 99.5%), NiO (Alfa Aesar, 98%) and V_2O_5 (Alfa Aesar, 99.6%).

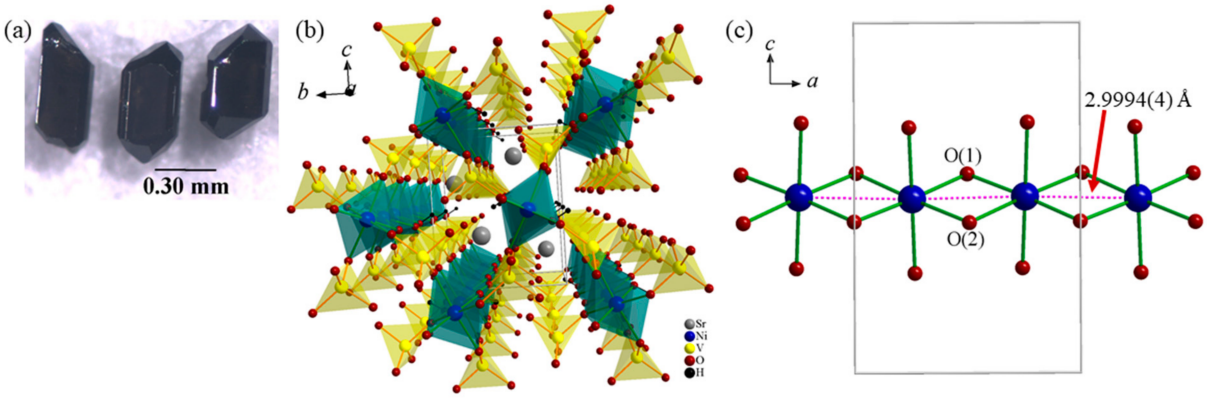

Figure 1. (**a**) Hydrothermally grown single crystals of SrNi(VO$_4$)(OH). (**b**) polyhedral view of SrNi(VO$_4$)(OH) viewed along *a*-axis. (**c**) The $Ni^{2+}O_6$ octahedra forms edged sharing chain which run parallel to *a*-axis.

2.2. Characterization

The single crystal structure was determined at room temperature using a Bruker D8 Venture diffractometer equipped with an Incoatec Mo Kα microfocus source and Photon 100 CMOS detector. Data collection and scaling were performed using the Apex3 software suite [38]. The structure was solved by direct methods using the SHELXTL software suite and refined on F^2 by least-squares, full-matrix techniques [39]. All non-hydrogen atoms were refined anisotropically. The difference electron density map was used to identify the hydrogen atom and its position constrained to prevent unreasonable variations in the O−H bond distance. Tables 1–3 report the crystallographic data, selected bond distances and angles and atomic coordinates and equivalent isotropic displacement parameters of SrNi(VO$_4$)(OH), respectively.

Table 1. Crystallographic data of SrNi(VO$_4$)(OH) determined by single crystal X-ray diffraction.

Empirical Formula	**SrNi(VO$_4$)(OH)**
formula weight (g/mol)	278.28
crystal system	orthorhombic
space group, *Z*	$P2_12_12_1$ (No. 19), 4
Crystal dimensions, mm	0.12 × 0.12 × 0.08

Table 1. *Cont.*

Empirical Formula	**$SrNi(VO_4)(OH)$**
T, K	298
a, Å	5.9952(4)
b, Å	7.5844(4)
c, Å	9.2240(5)
volume, $Å^3$	419.42(4)
D(calc), g/cm^3)	4.407
μ (Mo Kα), mm^{-1}	19.201
F(000)	520
Tmax, Tmin	1.0000, 0.7547
2θ range	2.27–30.52
reflections collected	16478
data/restraints/parameters	1284/1/79
final R [$I > 2\sigma(I)$] R_1, R_{w2}	0.0109, 0.0274
final R (all data) R_1, R_{w2}	0.0109, 0.0274
GoF	1.095
largest diff. peak/hole, $e/Å^3$	0.0416/−0.700

Table 2. Selected bond distances (Å) and angles (º) of $SrNi(VO_4)(OH)$.

$Ni(1)O_6$	
Ni(1)–O(1)	1.9659(1)
Ni(1)–O(1)	1.9763(2)
Ni(1)–O(2)	2.1226(2)
Ni(1)–O(2)	2.1678(1)
Ni(1)–O(3)	2.1422(2)
Ni(1)–O(4)	2.1353(2)
$V(1)O_4$	
V(1)–O(2)	1.7461(1)
V(1)–O(3)	1.7263(1)
V(1)–O(4)	1.7224(2)
V(1)–O(5)	1.6921(2)
O(2)–V(1)–O(3)	111.34(7)
O(2)–V(1)–O(4)	114.70(7)
O(2)–V(1)–O(5)	103.53(7)
O(3)–V(1)–O(4)	112.41(7)
O(3)–V(1)–O(5)	110.23(7)
O(4)–V(1)–O(5)	103.92(7)
Ni(1)–O(1)–Ni(1)	99.08(6)
Ni(1)–O(2)–Ni(1)	88.71(5)
Ni···Ni	2.9994(4)

Table 3. Fractional atomic coordinates and isotropic or equivalent isotropic displacement parameters (Å^2) of SrNi(VO_4)(OH) from single crystal X-ray data measured at room temperature.

Atom	*Wyckoff pos.*	*x*	*y*	*z*	*Ueq*
Sr(1)	4*a*	−0.02329(3)	0.13583(2)	0.16864(2)	0.00545(7)
Ni(1)	4*a*	0.24566(4)	−0.24437(4)	−0.00328(3)	0.00392(7)
V(1)	4*a*	−0.48981(6)	0.38778(4)	0.18885(3)	0.00274(7)
O(1)	4*a*	0.5019(2)	−0.1029(2)	−0.06759(1)	0.0049(3)
H(1)	4*a*	0.521(6)	0.001(4)	−0.017(3)	0.054(2)
O(2)	4*a*	−0.5077(3)	0.5668(2)	0.07041(1)	0.0058(3)
O(3)	4*a*	−0.7343(2)	0.3601(2)	0.28502(2)	0.0063(3)
O(4)	4*a*	−0.2581(2)	0.3883(2)	0.29928(2)	0.0065(3)
O(5)	4*a*	−0.4474(3)	0.2140(2)	0.07717(2)	0.0097(3)

2.3. Magnetization and Heat Capacity Measurements

The temperature-dependent magnetization and field-dependent magnetization measurements were performed using an array of small single crystals of SrNi(VO_4)(OH). These crystals were affixed to a quartz rod using GE varnish. Here, all the measurements were performed with the magnetic field along *a*-axis (Ni–O–Ni 1-D chain direction) and perpendicular to the *a*-axis. A total mass of 7.3 mg was used for the magnetization measurements, which were conducted using a SQUID magnetometer (Quantum Design, Magnetic Property Measurement System). A total mass of 1.8 mg was used for the heat capacity measurements. Heat capacity data were collected using the slope analysis technique as implemented in the Heat Capacity Option of the Quantum Design Physical Property Measurement System.

3. Results and Discussion

3.1. Synthesis and Structure of SrNi(VO_4)(OH)

SrNi(VO_4)(OH) belongs to the family of the adelite-descloizite mineral type. Their structures are similar but depending upon the chemistry of the parent compound, they tend to crystalize either in acentric space group $P2_12_12_1$ or centric *Pnma*. For example, naturally occurring adelite-mineral [CaMg(AsO_4)(OH)] crystallizes in $P2_12_12_1$ while descloizite-mineral [PbZn(VO_4)(OH)] crystallizes in *Pnma* [40,41]. The structure is made from two basic components, the 1-D *TM*–O–*TM* chains and the tetrahedral oxyanion groups. Since all atoms are in 4*d* sites, a vast array of combinations of oxyanions and metal cations can be accommodated. Therefore, the adelite-descloizite structure type represents an interesting example of an adaptable structure with capability of flexible chemical substitution at several different crystallographic sites [42]. Our previous work confirmed that the Sr*TM*(VO_4)(OH) series (*TM* = Mn, Co) belong to the adelite group in the acentric space group of $P2_12_12_1$ [14,15]. These structures play an important role since it consists of one-dimensional spin lattices and shows very interesting magnetic properties depending upon the spin state of the 1-D magnetic lattice. In continuation of hydrothermal synthesis of new transition metal-vanadates, we isolated another adelite-descloizite type structure, namely SrNi(VO_4)(OH) which is a new addition to the Sr*TM*(VO_4)(OH) series with an $S = 1$ magnetic state. The crystals grew in good quality and purity but unfortunately were not very large (~0.5mm). After the initial synthesis, reactions were optimized to try to achieve bigger crystals and a larger yield. However, crystal size did not improve despite multiple attempts using different synthesis reactions and parameters. Therefore, unlike the Mn and Co analogs, the crystals are too small to carry out single crystal neutron diffraction studies.

Hydrothermally grown single crystals of SrNi(VO_4)(OH) are presented in Figure 1a. The crystal structure of SrNi(VO_4)(OH) was investigated at 298 K using single crystal X-ray diffraction. The crystal structure of SrNi(VO_4)(OH) crystalizes in the previously described parent compound series of Sr*TM*(VO_4)(OH), $P2_12_12_1$ [14,15]. The orthorhombic

unit cell with the unit cell parameters of a = 5.9952(4) Å, b = 7.5844(4) Å, c = 9.2240(5) Å, V = 419.42(4) Å^3 was refined using the single crystal X-ray data. Sr^{2+}, Ni^{2+}, V^{5+} and O^{2-} are in 4*d* sites. Furthermore, our SXRD results confirmed that $SrNi(VO_4)(OH)$ is stoichiometric without any disorder and the crystal structure is presented in Figure 1. In Figure 1b, a partial polyhedral view of $SrNi(VO_4)(OH)$ is depicted along the *a*-axis to show the arrangement of 1D chains of Ni–O–Ni along the *a*-axis. These Ni–O–Ni chains are confined with VO_4-tetrahedral groups. Additionally, these VO_4 units interconnect Ni–O–Ni chains forming three-dimensional network. The Sr^{2+} occupies the channels made by NiO_6 and VO_4 units. As shown in Figure 1c NiO_6 octahedra forms edged sharing chains along the *a*-axis which are isolated by tetrahedral groups of VO_4, Figure 1b. As can be seen in Figure 1c, NiO_6 octahedral share edges through O(1) and O(2) to form $[Ni_2O_{10}]_\infty$ 1D chains. The V(1)O_4 tetrahedral groups connect to NiO_6 octahedra via axial oxygen, O(3) and O(4). Equatorial O(1) of NiO_6 connects directly to the hydrogen atom by forming OH^- group in the structure.

To understand the magnetic properties of the material, it is necessary to discuss the characteristic bond distance and angles of the $SrNi(VO_4)(OH)$ structure. The $Ni^{2+}-O$ bond distances range from 1.9659(1) to 2.1678(1) Å by forming highly distorted NiO_6-octahedra. The equatorial Ni–O bonds exhibit the largest distortion with an average Ni(1)–O(1) 1.9710(2) Å while the average of Ni(2)–O(2) is 2.1452(2) Å. Since O(1) and O(2) propagate in a zigzag pattern throughout the 1D chain, this distortion also propagates in the chain in a zigzag pattern. The axial Ni–O bonds also largely deviate from the expected sum of the Shannon crystal radii for 6-coordinate high spin Ni^{2+} and O^{2-}, which is 2.09 Å. Further, the Ni⋯Ni distances in the $[Ni_2O_{10}]_\infty$ chain is 2.9994(4) Å which is also somewhat smaller than previously reported Sr*TM*(VO4)(OH) structures, as expected. The Ni–O–Ni angles within the $[Ni_2O_{10}]_\infty$ chains range from 88.63° to 99.09°. Furthermore, the minimum distance between adjacent $[Ni_2O_{10}]_\infty$ chains is 5.9175(4) Å. Since these $[Ni_2O_{10}]_\infty$ chains are isolated by non-magnetic VO_4 units, more 1-D characteristics could be expected for $SrNi(VO_4)(OH)$ with competing intrachain and interchain interactions. The V–O bond distances are ranging from 1.6921(2) to 1.7461(1) Å with the average V–O bond distance of 1.7271 Å which is consistent with the expected sum of the Shannon crystal radii (1.73 Å) for a 4-coordinate V^{5+} and O^{2-}.

3.2. Magnetic Properties of SrNi(VO$_4$)(OH)

Results of the magnetization measurements are summarized in Figure 2. The anisotropic temperature dependence magnetic susceptibility is shown in Figure 2a. Here, magnetic measurements were performed with the applied magnetic field parallel to the Ni–O–Ni chain direction (*a*-axis) and perpendicular to the *a*-axis. At higher temperatures $T > 150$ K the magnetic susceptibility of the two different directions overlap with each other. The magnetic susceptibility follows a Curie–Weiss law at high temperature, demonstrated by the fit shown to the data above 150 K in Figure 2b using $M/H = C/(T - \Theta)$. Here, C is the Curie constant, which is a measure of the moment or spin of the magnetic ions, and Θ is the Weiss temperature, which is a measure of the strength of the magnetic interactions between ions [43]. The Curie constant is related to the spin S by $C = N_A g^2 \mu_B{}^2 S(S+1)/(3k_B)$, where N_A is Avogadro's number, g is the electron gyromagnetic ratio (=2.002), μ_B is the Bohr magneton, and k_B is the Boltzmann constant. We assume orbital angular moment is quenched. Since $(3k_B)/(N_A \mu_B{}^2)$ is very nearly 8, for an ion with spin S the molar Curie constant is given by $C = S(S+1)/2$ in units of cm^{3}K/mol. In $SrNi(VO_4)(OH)$, Ni^{2+} is in d^8 electron configuration with S = 1 state. The Curie–Weiss fitting resulted an effective moment of 2.8 μ_B/Ni and a Weiss temperature of 8 K. The effective magnetic moment of $SrNi(VO_4)(OH)$ agrees well with the calculated spin only magnetic moment of Ni^{2+} μ_{eff} = 2.8 μ_B/Ni. The positive Weiss temperature suggests that overall magnetic interactions are ferromagnetic. Furthermore, the characteristic broad maximum typical for 1-D antiferromagnetic spin chain systems is also suppressed. In general, the 1-D antiferromagnetic spin chains typically display a temperature dependence of their magnetic susceptibility resulting from the suppression

of the susceptibility at low temperatures as the magnetic correlations overcome thermal effects. Therefore, we can assume that $SrNi(VO_4)(OH)$ has dominant antiferromagnetic interactions even though it has a positive Weiss temperature from the fitting. This could be due to the strong interchain interactions which stabilize the overall AFM structure while intrachain interactions are ferromagnetic. Similar behavior has been observed previously for 1-D structures containing Co^{2+} (d^7) and Ni^{2+} (d^8) structures such as Na_4CoTeO_6 (θ = 2.3 K), Na_4NiTeO_6 (θ = 30 K), and $Ni_3(Mo_2O_8)(TeO_3)$ (θ = 15 K) indicating significant ferromagnetic interactions between magnetic centers within the 1-D chains [44,45]. To further clarify the nature of the magnetic properties of $SrNi(VO_4)(OH)$ detailed magnetic measurements and neutron scattering need to be carried out. Figure 2b inset shows the magnetic susceptibility measured at different magnetic fields 10–60 kOe with the applied magnetic field along the *a*-axis. With the increase of the applied magnetic field, the magnetic transition moves to lower temperatures and no clear field induced magnetic transition was observed. This suggests the presence of strong interchain antiferromagnetic interactions in $SrNi(VO_4)(OH)$. Comparisons can be made to isostructural magnetic compounds $SrMn(VO_4)(OH)$ and $SrCo(VO_4)(OH)$. The former was found to have antiferromagnetic chains of Mn^{2+} in a canted antiferromagnetic structure below T_N = 30 K including a broad hump in M/H near 80 K arising from one-dimensional magnetic correlations due to strong intrachain interactions [14]. In contrast, evidence of ferromagnetic intrachain correlations was recently observed in $SrCo(VO_4)(OH)$. Single crystal neutron diffraction confirms that the magnetic structure of $SrCo(VO_4)(OH)$ possesses 1-D ferromagnetic chains along the chain axis and each chain is compensated by an antiferromagnetic interaction between nearest neighbor chains generating a net antiferromagnetic magnetic structure. Additionally, $SrCo(VO_4)(OH)$ exhibits an interesting metamagnetic transition as well with a spin flip in a 2.8 kOe field [15]. Unlike $SrCo(VO_4)(OH)$ the nickel analog displays only a modest anisotropy (Figure 2a). Overall the general magnetic properties have some similarities and some differences to what we observed in $SrCo(VO_4)(OH)$. Single crystal neutron diffraction will be essential to confirm the magnetic structure of $SrNi(VO_4)(OH)$.

Figure 2c,d show the measured magnetic field dependence of the isothermal magnetization in two crystallographic orientations, respectively. Magnetization curves (Figure 2c,d) are linear near at room temperature as expected for a paramagnet. At 2 K, below the long-range ordering temperatures, some curvature is observed at higher field, H > 55 kOe when the applied magnetic field is along the *a*-axis. When the field is perpendicular the *a*-axis, isothermal magnetization at 2 K is more linear. This is likely associated with a spin-reorientation transition where Ni^{2+} canted moments can rotate towards the *a*-axis with the applied magnetic field. Similar spin-reorientation was observed for $SrCo(VO_4)(OH)$ [15]. Additionally, field-dependent heat capacity (Figure 3) shows C_P vs. T, where an anomaly can be seen around 8.2 K, which can be attributed to the phase transition near noted in the magnetization data. With the applied magnetic field, the heat capacity signal is suppressed while shifted to the lower temperatures which further confirms the presence of a spin re-orientation with the applied magnetic field. It can also be noted that the heat capacity peaks are somewhat broad and not of a pure λ type for a straightforward AFM type transition. Instead, the broad peaks again are suggestive of a 1-D magnetic chain with strong interchain coupling [46].

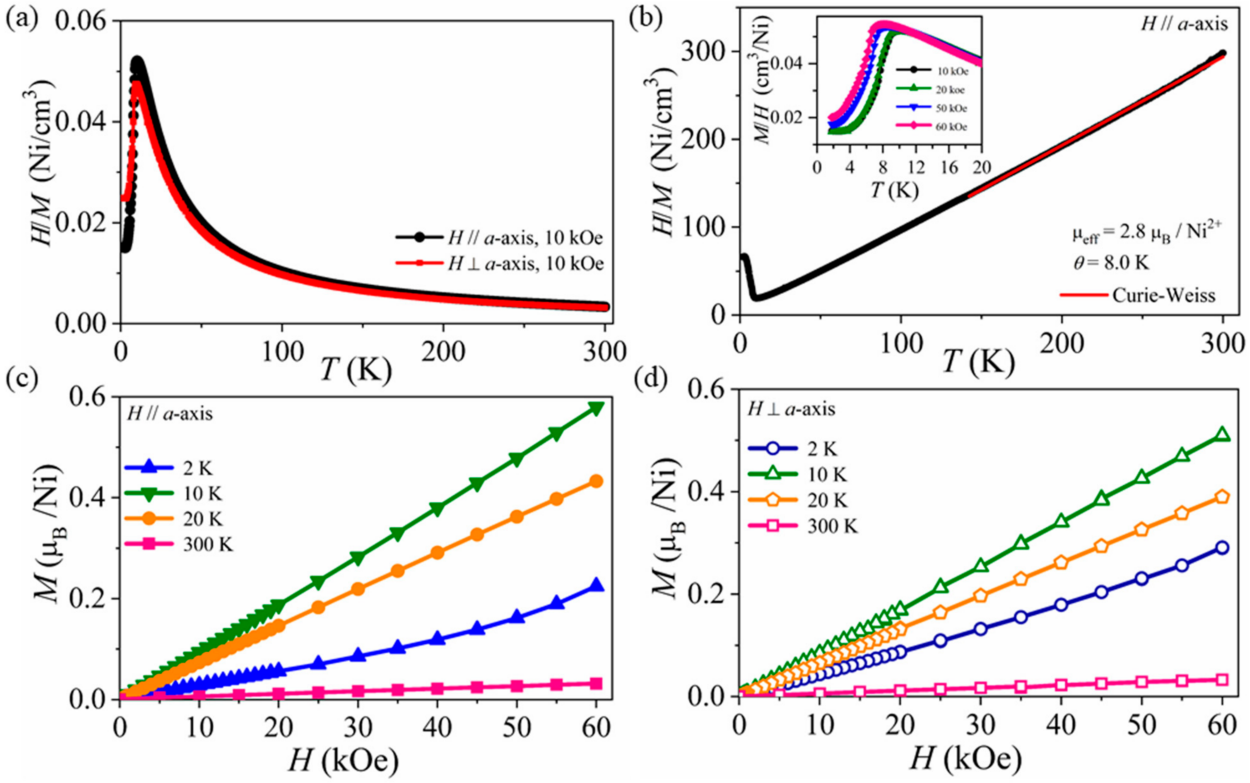

Figure 2. (**a**) Magnetic susceptibility (M/H) as a function of temperature at the applied magnetic field of 10 kOe along *a*-axis (solid black symbol) and perpendicular to the *a*-axis (solid red symbols). (**b**) Plot of the inverse susceptibility as a function of temperature and the linear Curie–Weiss fit. Inset: Field dependent of the magnetic susceptibility along the *a*-axis. (**c**,**d**) Isothermal magnetization curves measured at selected temperatures ranging from 2 K to 300 K for magnetic fields applied parallel to *a*-axis and perpendicular to the *a*-axis.

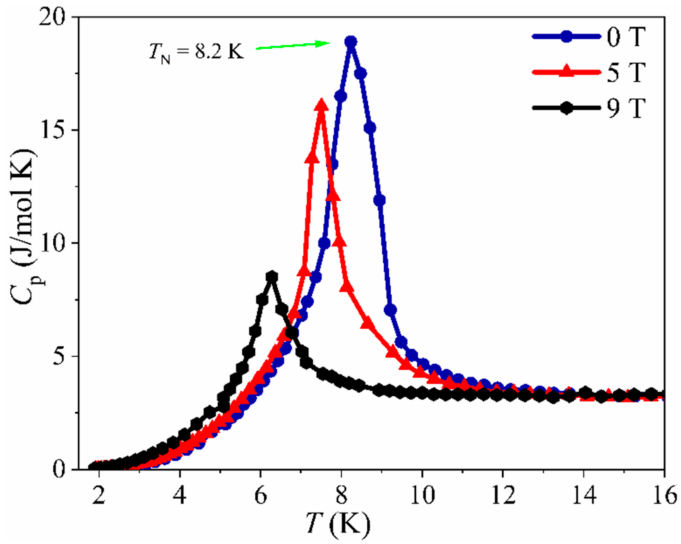

Figure 3. Heat capacity (Cp) measured for applied fields of 0, 5 and 9 T.

Neutron diffraction experiments and detailed anisotropic magnetization measurements (all three crystallographic directions) would be needed to gain the full insight into the magnetic ordering in this material. From the magnetization and heat capacity data we can conclude that the magnetic interactions and resulting magnetic order is FM along the chain direction, however, an AFM structure is ultimately stabilized below 8.2 K due to the strong interchain interactions. This is evidenced by the inference of both antiferromagnetic

and ferromagnetic correlations. These complexities of the magnetism of Sr*TM*(VO_4)(OH), *TM* = Mn, Co, Ni series likely arise from a combination of competing magnetic interactions, the low dimensional nature of the system, and the different spin states.

4. Summary and Conclusions

The continuing investigation of low dimensional chains of first row metal ions bridged by vanadate ions is reported herein. The research emphasizes the vital necesssity of high quality single crystal growth. The ability to prepare high quality large single crystals of various structural types of low dimensional chains relatively easily enables us to systematically vary the metal ion and hence the spin state. This allows us to probe complex magnetic behavior in a systematic fashion. In this case, we continue our investigation of the adelite-descloizite type compounds that contain isolated 1-D chains bridged by vanadate groups in several ways. Previous work demonstrates that SrMn(VO_4)(OH) with Mn^{2+} ($S = 5/2$) ions, displays canted antiferromagnetic structure below T_N = 30 K. Further, Dzyaloshinskii-Moriya antisymmetric exchange interaction produce a slight canting of the spins to give rise to a weak ferromagnetic component along the chain direction. On the other hand, magnetic properties and magnetic structure characterization of SrCo(VO_4)(OH) with S =3/2, confirm the ferromagnetic coupling of the Co moments along the *a*-axis and is compensated by significant antiferromagnetic interaction between nearest neighbor chains. In this paper single crystals of SrNi(VO_4)(OH) with S = 1, were synthesized using a high-temperature high-pressure hydrothermal method. The edge sharing quasi-octahedral chains separated from each other via VO_4 groups. Since these VO_4 units interconnect Ni–O–Ni 1-D chains, SrNi(VO_4)(OH) can be considered as a quasi 1-D system. Therefore, both intrachain and interchain interactions can be considered. Overall, the magnetic behavior suggests an antiferromagnetic behavior for SrNi(VO_4)(OH). However, Curie–Weiss fitting suggests that predominant interactions are ferromagnetic. This could be due to the competing AFM and FM interaction within the system where it forms 1-D ferromagnetic chains along the *a*-axis while they are compensated within the structure via interchain coupling to form a net antiferromagnetic structure.

Author Contributions: L.D.S. collected the data and wrote. T.M.S.P. and C.D.M. performed synthesis and data collections. K.T., T.H., H.K. and J.W.K. review and editing. All authors have read and agreed to the published version of the manuscript.

Funding: This work was supported in part by a University of Missouri Research Council Grant (Grant Number: URC-22-021). This work was also supported by a grant from the National Science Foundation (DMR-1808371 and DMR-2219129).

Data Availability Statement: CCDC 2203717 contain the supporting crystallographic data for this paper. These data can be obtained free of charge via www.ccdc.cam.ac.uk/data_request/cif (accessed on 25 August 2022), or by emailing data_request@ccdc.cam.ac.uk, or by contacting The Cambridge Crystallographic Data Centre, 12 Union Road, Cambridge CB2 1EZ, UK; fax: +44-1223-336033.

Acknowledgments: This research used resources at the Missouri University Research Reactor (MURR).

Conflicts of Interest: The authors declare no conflict of interest.

References

1. Chirayil, T.; Zavalij, P.Y.; Whittingham, M.S. Hydrothermal synthesis of vanadium oxides. *Chem. Mater.* **1998**, *10*, 2629–2640. [CrossRef]
2. Schindler, M.; Hawthorne, F.C.; Baur, W.H. A crystal-chemical approach to the composition and occurrence of vanadium minerals. *Can. Mineral.* **2000**, *38*, 1443–1456. [CrossRef]
3. Zavalij, P.Y.; Whittingham, M.S. Structural chemistry of vanadium oxides with open frameworks. *Acta Crystallogr. Sect. B Struct. Sci.* **1999**, *55*, 627–663. [CrossRef]
4. Amuneke, N.E.; Tapp, J.; de la Cruz, C.R.; Möller, A. Experimental realization of a unique class of compounds: XY-antiferromagnetic triangular lattices, $KAg_2Fe[VO_4]_2$ and $RbAg_2Fe[VO_4]_2$, with ferroelectric ground states. *Chem. Mater.* **2014**, *26*, 5930–5935. [CrossRef]

5. Reuss, A.; Ksenofontov, V.; Tapp, J.; Wulferding, D.; Lemmens, P.; Panthöfer, M.; Möller, A. Screw-type motion and its impact on cooperativity in $BaNa_2Fe[VO_4]_2$. *Inorg. Chem.* **2018**, *57*, 6300–6308. [CrossRef]
6. Yahia, H.B.; Gaudin, E.; Boulahya, K.; Darriet, J.; Son, W.-J.; Whangbo, M.H. Synthesis and characterization of the crystal structure and magnetic properties of the ternary manganese vanadate $NaMnVO_4$. *Inorg. Chem.* **2010**, *49*, 8578–8852. [CrossRef]
7. Koo, H.-J.; Whangbo, M.H.; Lee, K.-S. Investigation of the spin exchange interactions and magnetic structures of the $CrVO_4$-type transition metal phosphates, sulfates, and vanadates by spin dimer analysis. *Inorg. Chem.* **2003**, *42*, 5932–5937. [CrossRef]
8. Lawes, G.; Harris, A.B.; Kimura, T.; Rogado, N.; Cava, R.J.; Aharony, A.; Entin-Wohlman, O.; Yildirim, T.; Kenzelmann, M.; Broholm, C.; et al. Magnetically driven ferroelectric order in $Ni_3V_2O_8$. *Phys. Rev. Lett.* **2005**, *19*, 087205.
9. Sun, K.; Litvinchuk, A.P.; Tapp, J.; Lorenz, B.; Möller, A. $BaMn_9[VO_4]_6(OH)_2$: A unique canted antiferromagnet with a chiral "paddle-wheel" structural feature. *Inorg. Chem.* **2015**, *54*, 898–904. [CrossRef]
10. Chen, Y.; Lynn, J.W.; Huang, Q.; Woodward, F.M.; Yildirim, T.; Lawes, G.; Ramirez, A.P.; Rogado, N.; Cava, R.J.; Aharony, A.; et al. Complex magnetic order in the Kagomé staircase compound $Co_3V_2O_8$. *Phys. Rev. B* **2006**, *74*, 014430.
11. Clemens, O.; Rohrer, J.; Nénert, G. Magnetic structures of the low temperature phase of $Mn_3(VO_4)_2$—Towards understanding magnetic ordering between adjacent Kagomé layers. *Dalton Trans.* **2016**, *45*, 156–171. [CrossRef] [PubMed]
12. McMillen, C.D.; Kolis, J.W. Hydrothermal synthesis as a route to mineralogically-inspired structures. *Dalton Trans.* **2016**, *45*, 2772–2784. [PubMed]
13. Sanjeewa, L.D.; McGuire, M.A.; Garlea, V.O.; Hu, L.; Chumanov, G.; McMillen, C.D.; Kolis, J.W. Hydrothermal synthesis and characterization of novel brackebuschite-type transition metal vanadates: $Ba_2M(VO_4)_2(OH)$, $M = V^{3+}$, Mn^{3+}, and Fe^{3+}, with interesting Jahn−Teller and spin-liquid behavior. *Inorg. Chem.* **2015**, *54*, 7014–7020. [CrossRef] [PubMed]
14. Sanjeewa, L.D.; Garlea, O.V.; McGuire, M.A.; McMillen, C.D.; Cao, H.; Kolis, J.W. Structural and magnetic characterization of the one-dimensional S = 5/2 antiferromagnetic chain system $SrMn(VO_4)(OH)$. *Phys. Rev. B* **2016**, *93*, 224407. [CrossRef]
15. Sanjeewa, L.D.; Garlea, V.O.; McGuire, M.A.; Xing, J.; Cao, H.; Kolis, J.W.; Sefat, A.S. Observation of large magnetic anisotropy and field-induced magnetic state in $SrCo(VO_4)(OH)$: A structure with quasi one-dimensional magnetic chain. *Inorg. Chem.* **2020**, *59*, 1029–1037. [CrossRef]
16. Garlea, V.O.; Sanjeewa, L.D.; McGuire, M.A.; Batista, C.D.; Samarakoon, A.M.; Graf, D.; Winn, B.; Ye, F.; Hoffmann, C.; Kolis, J.W. Exotic magnetic field-induced spin-superstructures in a mixed honeycomb-triangular lattice system. *Phys. Rev. X* **2019**, *9*, 011038. [CrossRef]
17. Sanjeewa, L.D.; McMillen, C.D.; Willett, D.; Chumanov, G.; Kolis, J.W. Hydrothermal synthesis of single crystals of transition metal vanadates in the glaserite phase. *J. Solid State Chem.* **2016**, *236*, 61–68. [CrossRef]
18. Sanjeewa, L.D.; McMillen, C.D.; McGuire, M.A.; Kolis, J.W. Manganese vanadate chemistry in hydrothermal BaF_2 brines: $Ba_3Mn_2(V_2O_7)F_2$ and $Ba_7Mn_8O_2(VO_4)_2F_{23}$. *Inorg. Chem.* **2016**, *55*, 12512–12515. [CrossRef]
19. Sanjeewa, L.D.; McGuire, M.A.; McMillen, C.D.; Willett, D.; Chumanov, G.; Kolis, J.W. Honeycomb-like S = 5/2 spin lattices in new manganese(II) vanadates. *Inorg. Chem.* **2016**, *55*, 9240–9249. [CrossRef]
20. Yahne, D.R.; Sanjeewa, L.D.; Sefat, A.S.; Stadleman, B.; Kolis, J.W.; Calder, S.; Ross, K.A. Pseudo-spin versus magnetic dipole moment ordering in the isosceles triangular lattice material $K_3Er(VO_4)_2$. *Phy. Rev. B* **2020**, *102*, 104423. [CrossRef]
21. Pellizzeri, T.M.S.; Sanjeewa, L.D.; McMillen, C.D.; Garlea, V.O.; Ye, F.; Sefat, A.S.; Kolis, J.W. Single crystal neutron and magnetic measurements of $Rb_2Mn_3(VO_4)_2CO_3$ and $K_2Co_3(VO_4)_2CO_3$ with mixed honeycomb and triangular magnetic lattices. *Dalton Trans.* **2020**, *49*, 4323–4335. [CrossRef]
22. Sanjeewa, L.D.; McGuire, M.A.; McMillen, C.D.; Garlea, V.O.; Kolis, J.W. Polar materials with isolated V^{4+} $S = \frac{1}{2}$ triangles: $NaSr_2V_3O_3(Ge_4O_{13})Cl$ and $KSr_2V_3O_3(Ge_4O_{13})Cl$. *Chem. Mater.* **2017**, *29*, 1404–1412. [CrossRef]
23. Taddei, K.M.; Sanjeewa, L.D.; Xing, J.; Parker, D.; Podleznyak, A.; dela Cruz, C.; Sefat, A. Tunable Magnetic Order in Low-Symmetry SeO_3 Ligand Linked $TM_3(SeO_3)$ $3H_2O$ (*TM* = Mn, Co and Ni) Compounds. *Phy. Rev. M* **2020**, *4*, 024410. [CrossRef]
24. Erdei, S. Growth of oxygen deficiency-free YVO_4 single crystal by top-seeded solution growth technique. *J. Cryst. Growth.* **1993**, *134*, 1–13. [CrossRef]
25. Erdei, S.; Johnson, G.G.; Ainger, F.W. Growth studies of YVO_4 crystals (II). Changes in Y-V-O-stoichiometry. *Cryst. Res. Technol.* **1994**, *29*, 815–828. [CrossRef]
26. Sleight, A.W.; Ramirez, A.P. Disappearance of the metal-insulator transition in iridate pyrochlores on approaching the ideal $R_2Ir_2O_7$ stoichiometry. *Solid State Commun.* **2018**, *275*, 12–15. [CrossRef]
27. Sanjeewa, L.D.; Garlea, V.O.; McGuire, M.A.; McMillen, C.D.; Kolis, J.W. Magnetic ground state crossover in a series of glaserite systems with triangular magnetic lattices. *Inorg. Chem.* **2019**, *58*, 2813–2821. [CrossRef] [PubMed]
28. Sanjeewa, L.D.; Garlea, V.O.; McGuire, M.A.; Frontzek, M.; McMillen, C.D.; Fulle, K.; Kolis, J.W. Investigation of a structural phase transition and magnetic structure of $Na_2BaFe(VO_4)_2$: A triangular magnetic lattice with a ferromagnetic ground state. *Inorg. Chem.* **2017**, *56*, 14842–14849. [CrossRef]
29. Bera, A.K.; Lake, B.; Islam, A.T.M.N.; Klemke, B.; Faulhaber, E.; Law, J.M. Field-induced magnetic ordering and single-ion anisotropy in the quasi-one-dimensional Haldane chain compound $SrNi_2V_2O_8$: A single-crystal investigation. *Phys. Rev. B* **2013**, *87*, 224423. [CrossRef]
30. He, Z.; Fu, D.; Kyômen, T.; Taniyama, T.; Itoh, M. Crystal growth and magnetic properties of $BaCo_2V_2O_8$. *Chem. Mater.* **2005**, *17*, 2924–2926. [CrossRef]

31. Hong, S.; Burkhow, S.J.; Doughty, R.M.; Cheng, Y.; Ryan, B.J.; Mantravadi, A.; Roling, L.T.; Panthani, M.G.; Osterloh, F.E.; Smith, E.A.; et al. Local structural disorder in metavanadates MV_2O_6 (M = Zn and Cu) synthesized by the deep eutectic solvent route: Photoactive oxides with oxygen vacancies. *Chem. Mater.* **2021**, *33*, 1667–1682. [CrossRef]
32. Niesen, S.K.; Kolland, G.; Seher, M.; Breunig, O.; Valldor, M.; Braden, M.; Grenier, B.; Lorenz, T. Magnetic phase diagrams, domain switching, and quantum phase transition of the quasi-one-dimensional ising-like antiferromagnet $BaCo_2V_2O_8$. *Phys. Rev. B* **2013**, *87*, 224413. [CrossRef]
33. Ma, J.; Dela Cruz, C.D.; Hong, T.; Tian, W.; Aczel, A.A.; Chi, S.; Yan, J.-Q.; Dun, Z.L.; Zhou, H.D.; Matsuda, M. Magnetic phase transition in the low-dimensional compound $BaMn_2Si_2O_7$. *Phys. Rev. B* **2013**, *88*, 144405. [CrossRef]
34. Tsukada, I.; Sasago, Y.; Uchinokura, K.; Zheludev, A.; Maslov, S.; Shirane, G.; Kakurai, K.; Ressouche, E. $BaCu_2Si_2O_7$: A quasi-one-dimensional $S = 1/2$ antiferromagnetic chain system. *Phys. Rev. B* **1999**, *60*, 6601. [CrossRef]
35. Streltsov, S.V.; Khomskii, D.I. Electronic structure and magnetic properties of pyroxenes (Li, Na)TM(Si, Ge)$_2O_6$: Lowdimensional magnets with 90° bonds. *Phys. Rev. B Condens. Matter Mater. Phys.* **2008**, *77*, 064405. [CrossRef]
36. Millet, P.; Mila, F.; Zhang, F.C.; Mambrini, M.; Van Oosten, A.B.; Pashchenko, V.A.; Sulpice, A.; Stepanov, A. Biquadratic interactions and spin-peierls transition in the spin-1 chain $LiVGe_2O_6$. *Phys. Rev. Lett.* **1999**, *83*, 4176. [CrossRef]
37. Foley, J.; Hughes, A.; Lange, D. The atomic arrangement of brackbuschite redefined as $Pb_2(Mn^{3+},Fe^{3+})(VO_4)_2(OH)$ and comments on Mn+ octahedra. *Can. Mineral.* **1997**, *35*, 1027–1033.
38. *Apex3*; Bruker AXS Inc.: Madison, WI, USA, 2015; Available online: https://www.brukersupport.com/ProductDetail/3177 (accessed on 25 August 2022).
39. Sheldrick, G.M. A short history of SHELX. *Acta Crystallogr. Sect. A Found. Crystallogr.* **2008**, *64*, 112–122. [CrossRef]
40. Effenberger, H.; Krause, W.; Bernhardt, H.J. Structural investigations of adelite and cobaltaustinite, two members of the adelite-descloizite group Experimental Mineralogy. In Proceedings of the Ninth International Symposium on Experimental Mineralogy, Petrology and Geochemistry, Zurich, Switzerland, 24–27 March 2002; Volume 9, p. 30.
41. Hawthorne, F.C.; Faggiani, R. Refinement of the structure of descloizite. *Acta Cryst.* **1979**, *B35*, 717–720. [CrossRef]
42. Smit, J.P.; Stair, P.C.; Poeppelmeier, K.R. The adaptable lyonsite structure. *Chem. Eur. J.* **2006**, *12*, 5944–5953. [CrossRef]
43. Smart, J.S. *Effective Field Theories of Magnetism*; W.B. Saunders: Philadelphia, PA, USA, 1966.
44. He, Z.; Guo, W.; Cui, M.; Tang, Y. Synthesis and magnetic properties of new tellurate compounds Na_4MTeO_6 (M = Co and Ni) with a ferromagnetic spin-chain structure. *Dalton Trans.* **2017**, *46*, 5076. [CrossRef]
45. Jiang, H.; Xie, Z.; Mao, J. $Ni_3(Mo_2O_8)(XO_3)$ (X = Se, Te): The first nickel selenite- and tellurite-containing Mo_4 clusters. *Inorg. Chem.* **2007**, *46*, 6495–6501. [CrossRef]
46. Carlin, R.L. Magnetism and magnetic transitions of transition-metal compounds at low temperatures. *Acc. Chem. Res.* **1976**, *9*, 67–74. [CrossRef]